JACS
JOURNAL OF THE AMERICAN CHEMICAL SOCIETY
Communication
pubs.acs.org/JACS

Nanoscale Growth and Patterning of Inorganic Oxides Using DNA Nanostructure Templates

Sumedh P. Surwade,[†] Feng Zhou,[†] Bryan Wei,[‡,§] Wei Sun,[‡,§] Anna Powell,[†] Christina O'Donnell,[†] Peng Yin,*[,‡,§] and Haitao Liu*[,†]

[†]Department of Chemistry, University of Pittsburgh, Pittsburgh, Pennsylvania 15260, United States
[‡]Wyss Institute for Biologically Inspired Engineering, Harvard University, Boston, Massachusetts 02115, United States
[§]Department of Systems Biology, Harvard Medical School, Boston, Massachusetts 02115, United States

Supporting Information

ABSTRACT: We describe a method to form custom-shaped inorganic oxide nanostructures by using DNA nanostructure templates. We show that a DNA nanostructure can modulate the rate of chemical vapor deposition of SiO_2 and TiO_2 with nanometer-scale spatial resolution. The resulting oxide nanostructure inherits its shape from the DNA template. This method generates both positive-tone and negative-tone patterns on a wide range of substrates and is compatible with conventional silicon nanofabrication processes. Our result opens the door to the use of DNA nanostructures as general-purpose templates for high-resolution nanofabrication.

Recent advances in DNA nanotechnology make it possible to construct arbitrary-shaped DNA nanostructures at a theoretical precision down to 2 nm.[1−9] This level of shape control is unmatched by any other self-assembled material systems, such as block copolymers, self-assembled monolayers, and protein/peptide assemblies.[10−13] These DNA nanostructures can be deterministically deposited onto silicon wafers,[14−16] making them ideal templates for high-resolution nanofabrication.[4,12,14,15,17−28] Compared with competing top-down and bottom-up approaches for nanoscale patterning,[10−13] DNA-based nanofabrication could offer high throughput, high resolution, and potentially very low capital and operational costs: even with the current price of DNA synthesis, the cost of DNA template for patterning an area of 1 m^2 could be as low as $6.[17]

A major challenge in using a DNA nanostructure for nanoscale patterning involves transfer of its pattern to an inorganic substrate (e.g., a silicon wafer). Because of their limited chemical stability, DNA nanostructures are not compatible with the harsh chemical reaction conditions that are typically used to etch and deposit inorganic materials, such as KOH etching and plasma-assisted chemical vapor deposition (CVD). One approach to address this challenge is to deposit metal onto DNA via solution chemistry or vacuum evaporation.[18,22,23,26−29] However, existing approaches for DNA metallization typically produce nonconformal metal coatings, leading to a significant loss of resolution. DNA-mediated etching of SiO_2 was recently reported to transfer the pattern of a DNA origami to a SiO_2 substrate with ∼25 nm resolution.[20] However, this approach could only produce features with limited vertical contrast, typically 2−3 nm. There is an urgent need to develop pattern-transfer reactions that can offer high resolution, high contrast, and compatibility with both DNA nanotechnology and existing semiconductor nanofabrication processes.

Herein we report a shape-conserving, room-temperature CVD process to convert a DNA nanostructure into an inorganic oxide nanostructure of the same shape. Our method has a number of advantages compared with the early developments of area-selective CVD and the closely related area-selective atomic layer deposition (ALD). First of all, the shape of a DNA nanostructure is configurable, and the feature size can be as small as 2 nm. If the DNA nanostructure could be overcoated with a 1 nm thick layer of CVD-grown inorganic oxide, it should be possible to produce custom-shaped features with sub-5 nm resolution. In contrast, previous studies on area-selective CVD and ALD have mostly relied on photolithography to define the area for selective material deposition;[30−34] consequently, the resolution of these CVD-grown patterns was limited by that of the photolithography. Although in some cases chemically synthesized inorganic nanostructures (e.g., nanoparticles) have been used as templates,[35] they cannot produce custom-shaped patterns. Second, our approach can be carried out at room temperature and is compatible with DNA nanostructures and potentially many other self-assembled supramolecular assemblies. Third, and most importantly, our CVD method is the first to achieve selective deposition of inorganic oxide onto a DNA nanostructure in the presence of a SiO_2 substrate, and vice versa. Both DNA and SiO_2 are active substrates in traditional high-temperature CVD and ALD processes.[36] However, through control of the adsorption of water at room temperature, our CVD process is able to differentiate these two substrates and achieve selective deposition with nanometer-scale resolution.

Our CVD produces a conformal oxide coating on the DNA template. Since oxide is one of the most commonly used etching masks, this method opens the door to integrating DNA nanotechnology with modern nanofabrication processes. As an example, we have demonstrated deep anisotropic etching of a silicon wafer by using the CVD-grown oxide as a hard mask.

Received: February 19, 2013
Published: April 10, 2013

   dx.doi.org/10.1021/ja401785h | J. Am. Chem. Soc. 2013, 135, 6778−6781

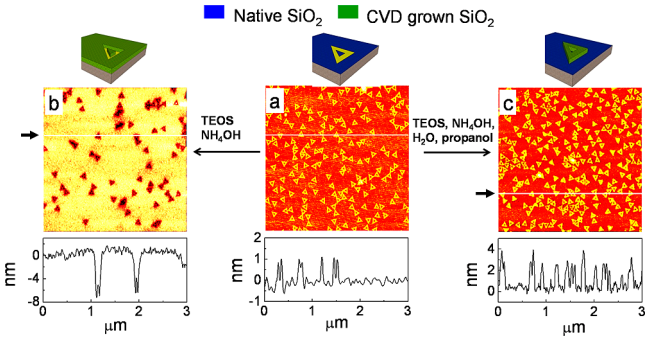

Figure 1. DNA-templated CVD growth of inorganic oxides. Cartoon representations (top), AFM images (middle), and AFM cross sections (bottom) are shown for (a) DNA origami triangles deposited on a Si substrate, (b) negative-tone triangular patterns obtained for CVD-grown SiO_2 (reaction time 12 h), and (c) positive-tone triangular patterns obtained for CVD-grown SiO_2 (reaction time 6 h).

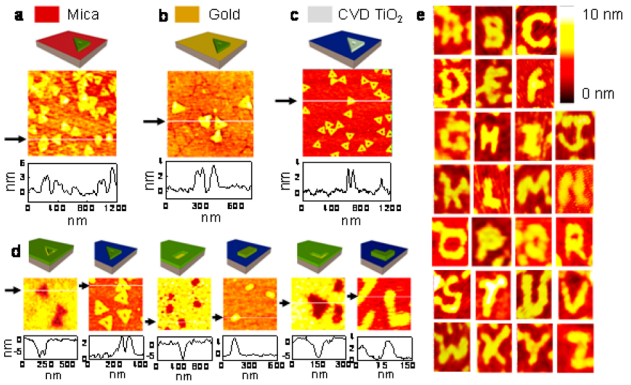

Figure 2. DNA-templated CVD growth of inorganic oxides of different shapes and substrates. (a–c) Cartoon representations (top), AFM images (middle), and AFM cross sections (bottom) of positive-tone triangular patterns of (a) CVD-grown SiO_2 on a mica substrate, (b) CVD-grown SiO_2 on a gold substrate, and (c) CVD-grown TiO_2 on a Si substrate. (d) Cartoons, high-resolution AFM images, and AFM cross sections of both positive-tone and negative-tone SiO_2 patterns on a silicon wafer templated by DNA nanostructures with three different shapes: triangle, rectangle, and L shape. (e) High-resolution AFM images (140 nm × 160 nm) of 26 positive-tone SiO_2 letters (A to Z) obtained using the corresponding DNA letters as templates. The arrows and white lines in (a–d) indicate the locations of the cross sections.

Figures 1 and 2 summarize our method for DNA-mediated CVD of oxide materials on various inorganic substrates. In a typical experiment, a DNA nanostructure is first deposited onto a substrate (e.g., Si wafer, mica, or gold). The CVD is carried out at room temperature in a closed glass chamber, inside which several liquid reservoirs deliver the CVD precursor and other required chemicals to the substrate through the gas phase. Both positive-tone and negative-tone patterns can be obtained. The detailed experimental procedure can be found in the Supporting Information (SI) (see Figures S1–S17).

Figure 1a shows an atomic force microscopy (AFM) image of triangular DNA templates deposited on a silicon wafer that has a thin layer (ca. 2 nm) of native oxide (also see Figure S1). The height and width of the edge of the DNA triangle were 1.2 ± 0.1 nm and 27 ± 1 nm, respectively (all reported width values are full widths at half-maximum; also see Table S1). When this sample was exposed to a mixed vapor of $Si(OEt)_4$ (TEOS), H_2O, and NH_3, deposition of SiO_2 occurred selectively on the SiO_2 surface that was not covered by the DNA template, resulting in a negative-tone pattern of SiO_2 (Figure 1b). The width of the trenches in Figure 1b was 42 ± 5 nm, while the depth was 7 ± 2 nm. The center void of the triangle template was retained in almost all of the structures, although with a reduced height contrast. To reverse the area selectivity of the CVD, we introduced propanol vapor and increased the relative humidity of the reaction chamber. In this case, the CVD reaction selectively deposited SiO_2 onto the DNA nanostructures to produce a positive-tone pattern (Figure 1c). After the CVD, the average height of the triangle structures increased from 1.2 ± 0.1 nm to 2.6 ± 0.5 nm while the width of the ridges increased from 27 ± 1 nm to 37 ± 3 nm. We note that the lateral dimension measured by AFM is likely limited by the tip–sample convolution effect and should be regarded as an upper limit. Nevertheless, faithful pattern transfer was clearly achieved for almost every DNA template under both positive-tone and negative-tone conditions. Our results contrast with those from previous work on metallization of DNA nanostructures, where the metal-plating process typically produced grainy and sometimes discontinuous metal nanostructures.[18,22,23,26–29]

This DNA-mediated CVD method is a versatile tool for general-purpose nanofabrication. First of all, the area-selective deposition of oxide materials is not limited to silicon wafer and can be extended to pattern other substrates. For example, Figure 2a,b shows the positive-tone CVD of SiO_2 onto DNA nanostructures deposited on mica and gold substrates, respectively (also see Figures S2, S3, S12, and S13). Second, oxide materials other than SiO_2 can also be deposited in a similar fashion by using suitable CVD precursors. For example, using titanium isopropoxide $[Ti(O^iPr)_4]$ as the precursor, we successfully produced positive-tone TiO_2 structures on a silicon wafer using the same triangular DNA templates (Figures 2c and S17). Finally, this CVD method is compatible with custom-shaped DNA templates. Figure 2d shows high-resolution AFM images of both positive-tone and negative-tone SiO_2 patterns templated by DNA nanostructures with three different shapes: triangle, rectangle, and L shape. Figure 2e shows high-resolution AFM images of positive-tone SiO_2 patterns templated by 26 letters constructed using the single-strand tiles (SST) approach.[1]

The chemical composition of the CVD-grown oxide nanostructures was confirmed by X-ray photoelectron spectroscopy (XPS) and energy-dispersive X-ray spectroscopy (EDX). For the XPS analysis, we used the SiO_2 triangle structures grown on a gold substrate because the other two substrates (silicon wafer and mica) contained silicon, which interfered with the data analysis. The XPS spectra (Figures S18 and S19) showed the presence of peaks for Si 2p (103.6 eV), Si 2s (154.8 eV), and O 1s (532.8 eV). The observed peak positions are consistent with the standard values for SiO_2.[37] XPS gave an Si:O ratio of 1:2.08 (or $SiO_{2.08}$), consistent with the deposition of SiO_2. EDX analysis of the CVD-grown SiO_2 triangles gave the expected Si and O peaks, while the TiO_2 structures gave the expected Ti and O peaks (Figure S20). Both the XPS and EDX spectra indicated the presence of carbon, which could arise from either the DNA or adsorption of CVD precursors and/or hydrocarbon contaminants in air. In addition to these spectroscopic characterizations, we also found that both the SiO_2 and TiO_2 structures could survive a 600 °C heating treatment in air, further confirming their inorganic nature (Figures S21 and S22).

dx.doi.org/10.1021/ja401785h | J. Am. Chem. Soc. 2013, 135, 6778–6781

a

$$Si(OC_2H_5)_4 + 2H_2O \xrightarrow{NH_3} SiO_2 + 4C_2H_5OH$$

b

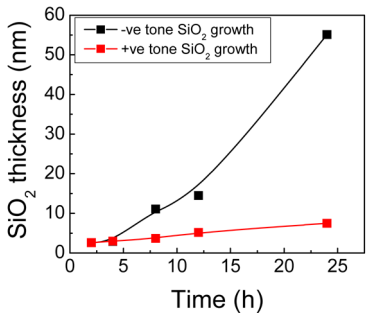

Figure 3. (a) Balanced chemical equation for the CVD of SiO_2 by hydrolysis of $Si(OEt)_4$ in the presence of NH_3 as a catalyst. (b) Temporal evolution of the average thickness (as measured by ellipsometry) of CVD-grown SiO_2 under positive-tone (red) and negative-tone (black) growth conditions. The lines are guide to the eye.

The key to achieving high-resolution area-selective CVD is to control the adsorption of water at the nanoscale. In our CVD process, the oxide precursors [$Si(OEt)_4$ and $Ti(OiPr)_4$] require water to hydrolyze (Figure 3a). In addition, NH_3 was used as a catalyst to enhance the reaction kinetics at room temperature.[38,39] Consequently, the rate of CVD should be closely related to the local concentration of adsorbed water and/or NH_3 catalyst. In the negative-tone CVD (Figure 1b), the Si/SiO_2 substrate was placed in the reaction chamber with two open vials, one containing CVD precursor and the other concentrated ammonia solution. Under these conditions, the SiO_2 CVD preferentially occurred on the existing SiO_2 surface, implying that SiO_2 is the preferred adsorption site for water and/or NH_3 under these conditions. In addition, one would also expect that the SiO_2 CVD should prefer to nucleate and grow onto an existing oxide surface. In this case, we used ellipsometry to track the average thickness of the oxide layer and observed a continuous increase in the oxide thickness from 2.6 nm (the thickness of the native oxide) to 14.5 nm after 12 h and 55.1 nm after 24 h (Figure 3b). Since the depth of the triangular trenches was 7 ± 2 nm after 12 h of reaction, we estimate that the deposition rate of CVD SiO_2 on the wafer surface was ca. 4 times faster than on the DNA nanostructures (see the SI for the detailed calculation).

To reverse the selectivity and achieve preferential oxide deposition onto the DNA nanostructure, it was necessary to decrease the activity of the SiO_2 surface and increase that of the DNA. We found that the former could be achieved by introducing *n*-propanol vapor into the CVD chamber. It has been shown that the coadsorption of *n*-propanol and water on a flat SiO_2 surface gives a binary adsorbate layer in which the adsorbed *n*-propanol molecules lie at the adsorbate−gas interface and water molecules are embedded underneath the *n*-propanol layer.[40] Although the detailed mechanism is still under investigation, we believe that under these conditions, the adsorbed water is not directly accessible to the CVD precursor, which should lead to significantly slower deposition of SiO_2 onto the flat SiO_2 surface. This prediction was indeed verified in our experiment: we saturated the CVD chamber with *n*-propanol vapor by introducing an open vial of *n*-propanol; in this case, we observed that the CVD still resulted in a negative-tone pattern transfer; however, the trenches were extremely shallow (<0.5 nm at 12 h; Figure S23), indicating a significant decrease (by a factor of at least 5) in the rate of SiO_2 deposition onto the flat SiO_2 surface. However, in this case, the DNA nanostructures still were not active toward SiO_2 CVD.

To increase the activity of the DNA nanostructures toward SiO_2 deposition, it was necessary to enhance their adsorption of water. This was achieved by introducing an additional open vial of water to increase the relative humidity inside the CVD chamber. Indeed, positive-tone pattern transfer was achieved when the above two efforts were combined. As shown in Figure 3b, in the presence of *n*-propanol vapor and increased relative humidity, the overall rate of SiO_2 deposition onto the wafer surface was still slow (ca. $^1/_{14}$ of that in the absence of *n*-propanol); however, in this case, AFM imaging showed a consistent increase in the height of the DNA nanostructures, which reached ∼7 nm at 24 h (Figure S14). From both the AFM and ellipsometry data, we estimate that the rate of SiO_2 CVD onto DNA was at least 2.6 times faster than onto the wafer surface (see the SI for the detailed calculation).

The formation of both positive-tone and negative-tone patterns is kinetically controlled. Because CVD-grown oxide is deposited conformally, the quality of the pattern transfer deteriorates, and fine features are lost at long reaction times. For example, after 24 h of reaction, the negative-tone SiO_2 patterns disappeared completely (Figure S8) while the positive-tone patterns lost the central void feature and became solid triangles (Figure S14).

Water adsorption also explains the behavior of different substrates in our CVD process. For example, we found that only positive-tone growth could be achieved for DNA triangles deposited on a gold substrate, even under conditions that produced a negative-tone pattern on a Si wafer (Figures S7 and S10). This observation is consistent with the chemical inertness of gold, which does not allow water and ammonia to adsorb strongly on its surface.[41] For a mica substrate, the contrast of the negative-tone pattern was very small, presumably because of the very small difference in the adsorption isotherms of water on DNA and mica.[42,43]

The SiO_2 nanostructure produced by our CVD process can be used as a hard mask for etching the underlying silicon substrates. In fact, SiO_2 is one of the most often used masks in silicon nanofabrication. To demonstrate this feasibility, we carried out deep anisotropic etching of silicon using the CVD-grown SiO_2 as a hard mask (Figure 4). Briefly, we deposited DNA triangles onto a silicon [110] wafer and grew a negative-tone SiO_2 pattern. The wafer was then exposed to a SF_6/O_2 plasma that selectively etches Si but not SiO_2.[44] After the plasma etching, we removed the CVD-grown SiO_2 mask with hydrofluoric acid (HF) to expose the underlying silicon. AFM imaging of the wafer revealed triangular trenches on the surface, indicating successful pattern transfer to the silicon layer. As shown in Figure 4, the depth of the trenches was 25 ± 2 nm, while the width was 55 ± 3 nm. For comparison, the depth and width of the trenches of the CVD-grown SiO_2 mask were 7 ± 2 and 42 ± 5 nm, respectively. Almost all of the triangles showed the center void feature, although with a reduced vertical contrast. The silicon surface was rough, which we believe to be a result of the amorphous nature of the SiO_2 grown under our current CVD process.

In conclusion, we have developed a novel approach to pattern custom-shaped inorganic oxide nanostructures by using a DNA nanostructure template. Our area-selective CVD method converts a DNA nanostructure into an oxide one,

dx.doi.org/10.1021/ja401785h | J. Am. Chem. Soc. 2013, 135, 6778−6781

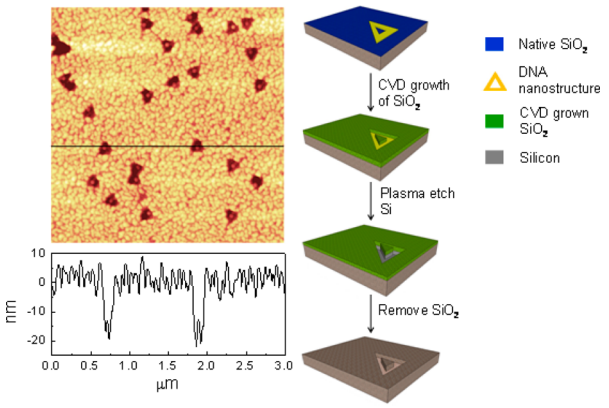

Figure 4. (left) AFM image and cross section of triangular trenches obtained by SF_6/O_2 plasma etching of a Si substrate using a negative-tone CVD-grown SiO_2 as a hard mask. The black line indicates the location of the cross section. (right) Schematic illustration of the use of a DNA nanostructure to pattern silicon.

which can be used as a hard mask for conventional semiconductor nanofabrication. Recently, two studies have demonstrated the deterministic deposition of DNA nanostructures on a silicon wafer.[14,15] This advance, together with our results described here, opens up the possibility to integrate DNA nanotechnology with conventional nanolithography to create high-resolution patterns. Although the resolution demonstrated here cannot yet compete with that of the best extreme UV lithography and electron-beam lithography, our approach is parallel, high-throughput and has the potential to drastically reduce the capital investment and operational cost of high-resolution (<20 nm) nanofabrication.[17]

■ ASSOCIATED CONTENT

Supporting Information

Experimental details, additional figures, and a table. This material is available free of charge via the Internet at http://pubs.acs.org.

■ AUTHOR INFORMATION

Corresponding Author

hliu@pitt.edu; peng_yin@hms.harvard.edu

Notes

The authors declare no competing financial interest.

■ ACKNOWLEDGMENTS

H.L. acknowledges financial support from AFOSR Young Investigator Program (FA9550-13-1-0083), the Mascaro Center for Sustainable Innovation, and the Central Research Development Fund of the University of Pittsburgh. The work is also supported by a DARPA Young Faculty Award N66001-11-1-4136, an ONR Young Investigator Program Award N000141110914, an ONR Grant N000141010827 and an NSF CAREER Award CCF1054898 to P.Y.

■ REFERENCES

(1) Wei, B.; Dai, M. J.; Yin, P. *Nature* **2012**, *485*, 623.
(2) Pinheiro, A. V.; Han, D.; Shih, W. M.; Yan, H. *Nat. Nanotechnol.* **2011**, *6*, 763.
(3) Han, D.; Pal, S.; Nangreave, J.; Deng, Z.; Liu, Y.; Yan, H. *Science* **2011**, *332*, 342.
(4) Sharma, J.; Chhabra, R.; Cheng, A.; Brownell, J.; Liu, Y.; Yan, H. *Science* **2009**, *323*, 112.
(5) Endo, M.; Sugiyama, H. *ChemBioChem* **2009**, *10*, 2420.
(6) Douglas, S. M.; Dietz, H.; Liedl, T.; Hogberg, B.; Graf, F.; Shih, W. M. *Nature* **2009**, *459*, 414.
(7) Dietz, H.; Douglas, S. M.; Shih, W. M. *Science* **2009**, *325*, 725.
(8) Rothemund, P. W. *Nature* **2006**, *440*, 297.
(9) Ke, Y.; Ong, L. L.; Shih, W. M.; Yin, P. *Science* **2012**, *338*, 1177.
(10) Gazit, E. *Chem. Soc. Rev.* **2007**, *36*, 1263.
(11) Hawker, C. J.; Russell, T. P. *MRS Bull.* **2005**, *30*, 952.
(12) Yan, H.; Park, S. H.; Finkelstein, G.; Reif, J. H.; LaBean, T. H. *Science* **2003**, *301*, 1882.
(13) Xia, Y.; Whitesides, G. M. *Angew. Chem., Int. Ed.* **1998**, *37*, 550.
(14) Hung, A. M.; Micheel, C. M.; Bozano, L. D.; Osterbur, L. W.; Wallraff, G. M.; Cha, J. N. *Nat. Nanotechnol.* **2010**, *5*, 121.
(15) Kershner, R. J.; Bozano, L. D.; Micheel, C. M.; Hung, A. M.; Fornof, A. R.; Cha, J. N.; Rettner, C. T.; Bersani, M.; Frommer, J.; Rothemund, P. W. K.; Wallraff, G. M. *Nat. Nanotechnol.* **2009**, *4*, 557.
(16) Gao, B.; Sarveswaran, K.; Bernstein, G. H.; Lieberman, M. *Langmuir* **2010**, *26*, 12680.
(17) Zhang, G.; Surwade, S. P.; Zhou, F.; Liu, H. *Chem. Soc. Rev.* **2013**, *42*, 2488.
(18) Pearson, A. C.; Liu, J.; Pound, E.; Uprety, B.; Woolley, A. T.; Davis, R. C.; Harb, J. N. *J. Phys. Chem. B* **2012**, *116*, 10551.
(19) Kuzyk, A.; Schreiber, R.; Fan, Z.; Pardatscher, G.; Roller, E. M.; Hogele, A.; Simmel, F. C.; Govorov, A. O.; Liedl, T. *Nature* **2012**, *483*, 311.
(20) Surwade, S. P.; Zhao, S.; Liu, H. *J. Am. Chem. Soc.* **2011**, *133*, 11868.
(21) Schreiber, R.; Kempter, S.; Holler, S.; Schuller, V.; Schiffels, D.; Simmel, S. S.; Nickels, P. C.; Liedl, T. *Small* **2011**, *7*, 1795.
(22) Puchkova, A. O.; Sokolov, P.; Petrov, Y. V.; Kasyanenko, N. A. *J. Nanopart. Res.* **2011**, *13*, 3633.
(23) Geng, Y.; Liu, J.; Pound, E.; Gyawali, S.; Harb, J. N.; Woolley, A. T. *J. Mater. Chem.* **2011**, *21*, 12126.
(24) Li, H.; Carter, J. D.; La Bean, T. H. *Mater. Today* **2009**, *12*, 24.
(25) Becerril, H. A.; Woolley, A. T. *Chem. Soc. Rev.* **2009**, *38*, 329.
(26) Becerril, H. A.; Woolley, A. T. *Small* **2007**, *3*, 1534.
(27) Hulme, J. P.; Gwak, J.; Miyahara, Y. *J. Am. Chem. Soc.* **2006**, *128*, 390.
(28) Deng, Z.; Mao, C. *Angew. Chem., Int. Ed.* **2004**, *43*, 4068.
(29) Kim, H. J.; Roh, Y.; Hong, B. *Langmuir* **2010**, *26*, 18315.
(30) Jiang, X.; Bent, S. F. *J. Phys. Chem. C* **2009**, *113*, 17613.
(31) Farm, E.; Kemell, M.; Ritala, M.; Leskela, M. *J. Phys. Chem. C* **2008**, *112*, 15791.
(32) Lee, J. P.; Sung, M. M. *J. Am. Chem. Soc.* **2004**, *126*, 28.
(33) Walker, A. V. *Langmuir* **2010**, *26*, 13778.
(34) Hampden-Smith, M. J.; Kodas, T. T. *Chem. Vap. Deposition* **1995**, *1*, 39.
(35) Weber, M. J.; Mackus, A. J. M.; Verheijen, M. A.; van der Marel, C.; Kessels, W. M. M. *Chem. Mater.* **2012**, *24*, 2973.
(36) Lu, Y.; Bangsaruntip, S.; Wang, X.; Zhang, L.; Nishi, Y.; Dai, H. *J. Am. Chem. Soc.* **2006**, *128*, 3518.
(37) Naumkin, A. V.; Kraut-Vass, A.; Powell, C. J. *NIST X-ray Photoelectron Spectroscopy Database*; NIST Standard Reference Database 20, version 3.5; http://srdata.nist.gov/xps/Default.aspx.
(38) Klaus, J. W.; George, S. M. *J. Electrochem. Soc.* **2000**, *147*, 2658.
(39) Deng, X.; Mammen, L.; Butt, H.-J.; Vollmer, D. *Science* **2012**, *335*, 67.
(40) Barnette, A. L.; Kim, S. H. *J. Phys. Chem. C* **2012**, *116*, 9909.
(41) Kay, B. D.; Lykke, K. R.; Creighton, J. R.; Ward, S. J. *J. Chem. Phys.* **1989**, *91*, 5120.
(42) Malani, A.; Ayappa, K. G. *J. Phys. Chem. B* **2009**, *113*, 1058.
(43) Balkose, D.; Alp, B.; Ulku, S. *J. Therm. Anal. Calorim.* **2008**, *94*, 695.
(44) Tzeng, Y.; Lin, T. H. *J. Electrochem. Soc.* **1987**, *134*, 2304.